ANODIC BEHAVIOR OF InP: FILM GROWTH, POROUS STRUCTURES AND CURRENT OSCILLATIONS

D.N. Buckley[†‡], C. O'Dwyer[†‡], E. Harvey[†]*, T. Melly[†‡],
M. Serantoni[‡], D. Sutton[‡], and S.B. Newcomb[‡]

[†]*Department of Physics, University of Limerick, Ireland*
[‡]*Materials & Surface Science Institute, University of Limerick, Ireland*
**present address Hewlett-Packard, Leixlip, Co. Kildare, Ireland*

ABSTRACT

We review our recent work on the anodization of InP in KOH electrolytes. The anodic oxidation processes are shown to be remarkably different in different concentrations of KOH. Anodization in 2 - 5 mol dm^{-3} KOH electrolytes results in the formation of porous InP layers but, under similar conditions in a 1 mol dm^{-3} KOH, no porous structure is evident. Rather, the InP electrode is covered with a thin, compact surface film at lower potentials and, at higher potentials, a highly porous surface film is formed which cracks on drying. Anodization of electrodes in 2 - 5 mol dm^{-3} KOH results in the formation of porous InP under both potential sweep and constant potential conditions. The porosity is estimated at ~65%. A thin layer (~ 30 nm) close to the surface appears to be unmodified. It is observed that this dense, near-surface layer is penetrated by a low density of pores which appear to connected it to the electrolyte. Well-defined oscillations are observed when InP is anodized in both the KOH and $(NH_4)_2S$. The charge per cycle remains constant at 0.32 C cm^{-2} in $(NH_4)_2S$ but increases linearly with potential in KOH. Although the characteristics of the oscillations in the two systems differ, both show reproducible and well-behaved values of charge per cycle.

INTRODUCTION

III-V semiconductors are widely used in optoelectronic devices as well as in high power and high speed electronic devices. Studies of the anodic growth of films on III-V semiconductors such as InP [1] and GaAs [2] have stemmed from their potential use as passivation layers and as insulating layers in devices. The nature of the anodic film formed is very dependant on the details of the electrochemical procedure. For example anodic treatments on InP in sulphur-containing electrolytes can result in passivated surfaces with increased stability [3,4] or thicker porous films in which cracking of the anodically grown surface film occurs [5-8]. Photoluminescence measurements of photo-anodically grown films on GaN have indicated the passivating nature of the layers [9] grown and metal-oxide-semiconductor (MOS) structures using photo-electrochemically formed oxide layers on GaN have been fabricated [10]. However, depending on the anodization details, cracking of the anodic oxide film can also occur for the case of GaN. [9]

Pore formation on Ge [10], InP [11], GaAs [12], GaP [13,14], and SiC [15] has been studied during potentiostatic or galvanostatic anodisation in acidic solution. The pronounced anisotropy of these compounds with respect to etching [16] makes them potential candidates for the formation of photonic crystals, particularly if ordered arrays of parallel pores can be created. Anion type and concentration can play a significant role in affecting the pore growth and morphology [17,18]. The depths of porous layers and their preferential crystallographic growth directions have been shown to be affected by the substrate type [19], orientation [20] and doping density [21].

In this paper, we review our recent work on the anodization of InP in KOH electrolytes. The formation of porous InP and anodic oxide films is discussed. Characteristic current oscillations are described and compared with the behavior observed in $(NH_4)_2S$ electrolytes.

EXPERIMENTAL

The working electrode consisted of polished (100)-oriented monocrystalline sulphur doped n-InP with a carrier concentration of approximately 3×10^{18} cm^{-3}. An ohmic contact was made by alloying indium to the InP sample and the contact was isolated from the electrolyte by means of a suitable varnish. The electrode area was typically 0.2 cm^2. Anodization was carried out in KOH electrolytes varying in concentration from 1 – 5 mol dm^{-3}. A conventional three electrode configuration was used employing a platinum counter electrode and saturated calomel reference electrode (SCE) to which all potentials are referenced. Prior to immersion in the electrolyte, the working electrode was dipped in a 3:1:1 H_2SO_4:H_2O_2:H_2O etchant and rinsed in deionized water. All of the electrochemical experiments were carried out at room temperature and in the dark.

A CH Instruments Model 650A Electrochemical Workstation interfaced to a Personal Computer (PC) was employed for cell parameter control and for data acquisition. Ellipsometric measurements of thin surface films were made with a J.A. Wollam M2000 Spectroscopic Ellipsometer. The surfaces of the anodized samples were examined using a Joel JSM 840 scanning electron microscope (SEM). Cross-sectional slices were thinned to electron transparency using standard focused ion beam milling procedures by means of a FEI 200 FIBSIMS workstation. The transmission electron microscopy (TEM) and electron diffraction was performed using a JEOL 2010 TEM operating at 200 kV. A Princeton Gamma-Tech digital spectrometer was used with the SEM for Energy Dispersive X-ray analysis (EDX).

RESULTS AND DISCUSSION

Cross-sectional TEM micrographs of n-InP electrodes subjected to a potential sweep a scan rate of 2.5 mV s^{-1} in KOH are shown in Fig 1. The electrode in Fig. 1a was scanned in 3 mol dm^{-3} KOH from 0 V to 0.68 while the electrode in Fig. 1b was scanned in 1 mol dm^{-3} KOH from 0 V to 1.3 V. It is evident that the anodic oxidation processes are remarkably different in the two different concentrations of KOH. Anodization in 3 mol dm^{-3} KOH electrolytes results in the formation of porous InP layers. The layer typically extends over 750 nm into the bulk substrate and there is no observable oxide

film present on the surface, although TEM electron diffraction measurements indicate that In_2O_3 exists within the pores [11]. Similar porous layers are obtained in 2 mol dm^{-3} and 5 mol dm^{-3} KOH.

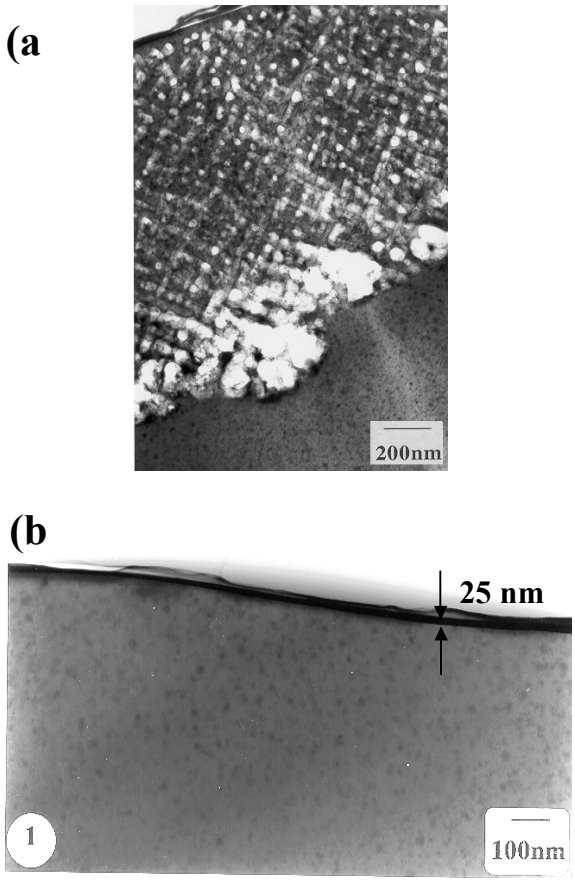

Fig. 1 Bright field through focal TEM micrographs of InP electrode cross-sections after a potential sweep from (a) 0.0 V to 0.68 V (SCE) at a scan rate of 2.5 mV s^{-1} in 3 mol dm^{-3} KOH and (b) 0.0 V to 1.3 V at a scan rate of 10 mV s^{-1} in 1 mol dm^{-3} KOH.

In contrast, after a similar potential sweep in a 1 mol dm^{-3} KOH electrolyte no porous structure is evident on the electrode; rather the InP electrode is covered with a relatively compact surface film with a thickness of ~25 nm as indicated in Fig. 1b. Electron diffraction data obtained for the surface film, indicates that it is predominantly In_2O_3 with some $InPO_4$. This is in agreement with previous reports on the composition of anodic films on InP [1,22].

Behavior in 1 mol dm^{-3} KOH: Surface Film Formation.

Fig. 2 shows linear sweep voltammograms of InP electrodes in 1 mol dm^{-3} KOH for a series of scan rates in the range 2.5 mV s^{-1} to 10 mV s^{-1}. The potential was scanned from 0.0 V to 2.5 V (SCE) in each case. The shape of the curves is similar for all scan rates. The peak current density increases relatively little (~50% over the range) with increasing scan rate and potential at the peak shifts slightly to less anodic values.

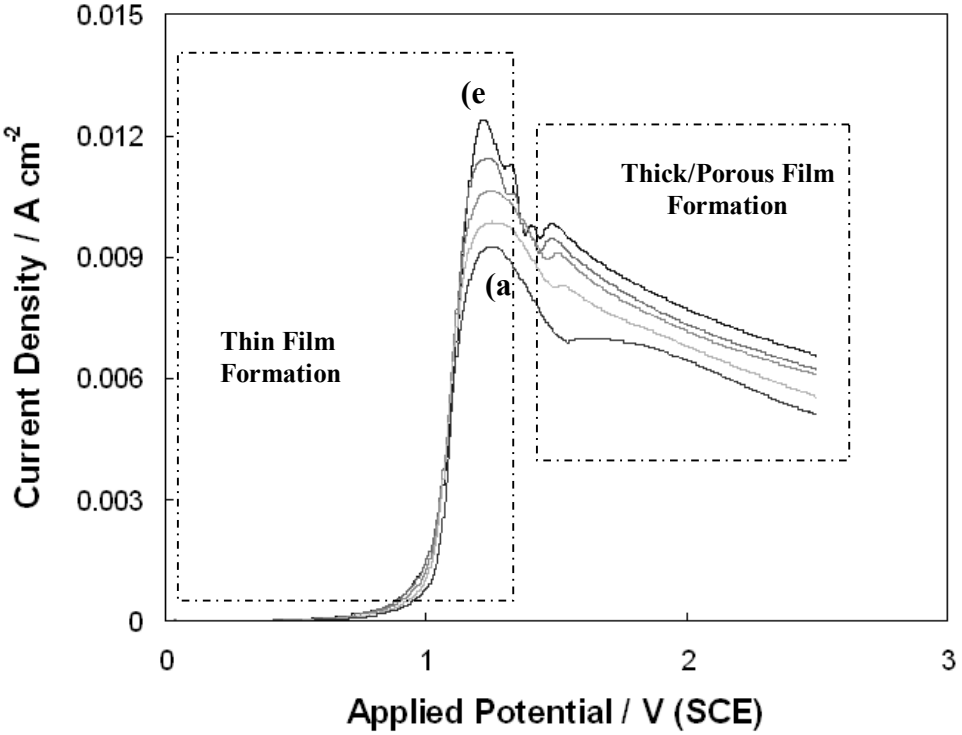

Fig. 2 Linear potential sweeps of InP electrodes in 1 mol dm^{-3} KOH solution from 0.0 V to 2.5 V (SCE) at scan rates of (a) 2.5 mV s^{-1}, (b) 3.75 mV s^{-1}, (c) 5 mV s^{-1}, (d) 7.5 mV s^{-1} and (e) 10 mV s^{-1}.

The thickness of the surface film formed was estimated by spectroscopic ellipsometry measurements for potential sweeps to values in the range 0.6 – 1.3 V. It was found to increase gradually, reaching a value of ~27 nm at the highest potential examined (1.3 V) and this value is in reasonable agreement with the film thickness as measured using TEM (~25 nm). At higher potentials, a surface film was formed which appeared cracked when examined by optical and scanning electron microscopy.

To investigate the origin of cracking in these films, an n-InP electrode was subjected to a linear potential sweep between 0.0 V and 2.5 V. Following this anodization, the electrode was rinsed in deionized water and quickly transferred while still wet to a container in which the relative humidity was maintained at approximately 100% in order to prevent it from drying while being transported to the microscope. The sample was then quickly transferred from the container to the optical microscope stage and immediately examined. A time sequence of images obtained as the sample was allowed to dry in ambient laboratory air is shown in Fig. 3. The first image obtained (Fig. 3(a)) shows that initially the surface was essentially featureless at this magnification, with no evidence of surface cracking. However, after ~4 minutes, cracks had appeared in the film (just discernable in Fig 3(c) and clearly visible in Fig. 3(d)). In Fig. 3(e), taken a few minutes later, further cracks are seen to have developed and it is also seen that existing cracks had broadened. The progression of film cracking was monitored over a period ~22 minutes and it is obvious from the images in Fig. 3(a) through 3(h) taken over this time period that crack formation and broadening continued as the sample was allowed to dry.

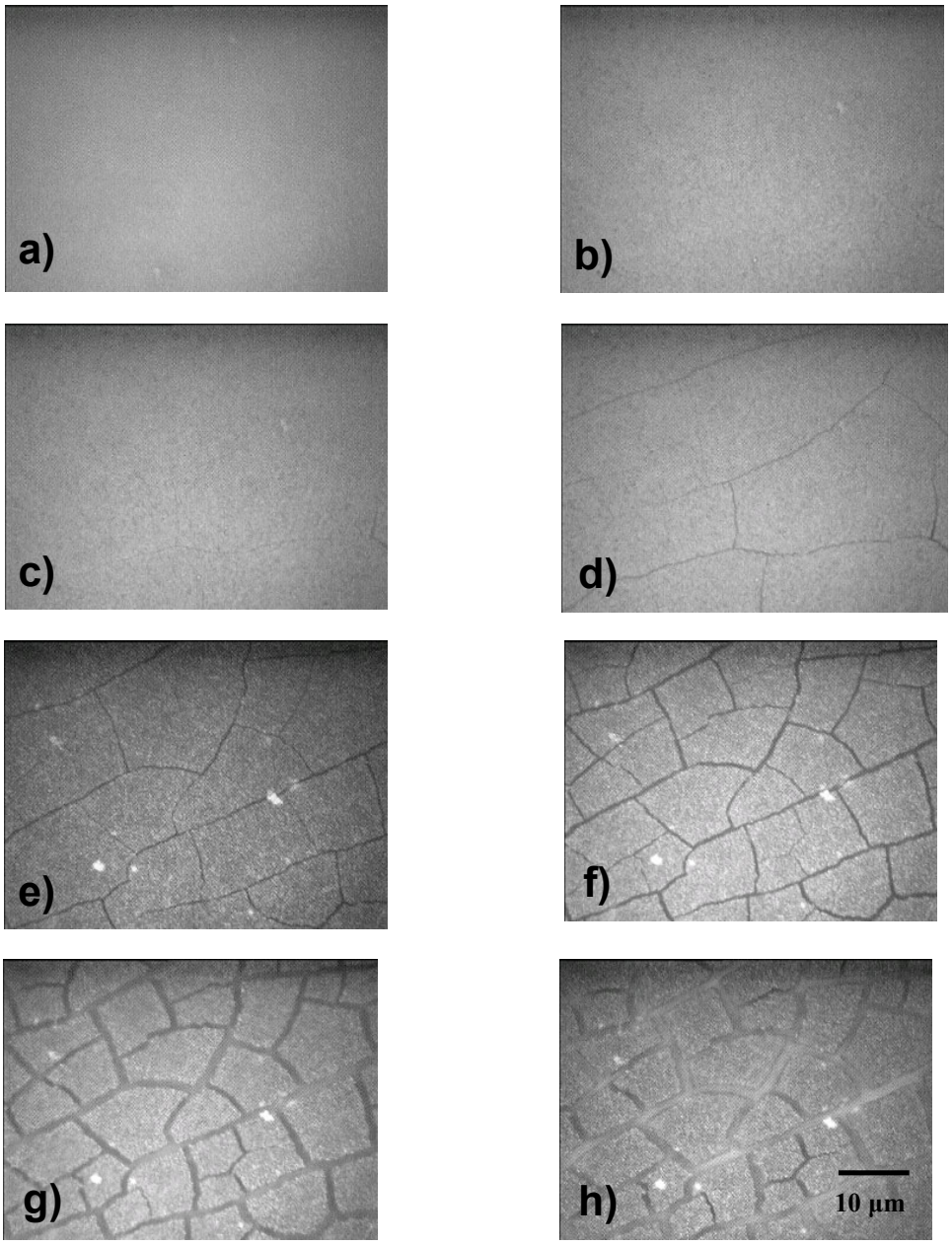

Figure 3. Time-lapse sequence of optical micrographs showing the evolution of surface cracks on a film as it dries: (a) through (h) were taken sequentially over a period of ~22 minutes. The film was formed by subjecting an n-InP electrode to a linear potential sweep from 0.0 V and 2.5 V in 1 mol dm^{-3} KOH at a scan rate of 2.5 mV s^{-1}.

These observations reveal valuable information on how and when the cracking of the surface film occurs. Thus we attribute the crack formation to shrinkage of the film as it dries. Similar results have been obtained for InP in 3 mol dm^{-3} $(NH_4)_2S$. In both cases, the film is highly porous in nature and this property of the film is expected to enhance the shrinkage when water is lost by evaporation. The surface cracking is not characteristic of

the film *in-situ* during the anodization procedure but rather occurs after the electrode has been removed from the electrolyte and allowed to dry (*ex-situ*).

Behavior in Higher Concentrations of KOH: Porous InP Formation.

Linear sweep voltammograms of InP electrodes in 3 mol dm^{-3} KOH are shown in Fig. 4 for a series of scan rates in the range 1 mV s^{-1} to 10 mV s^{-1}. Similar curves are

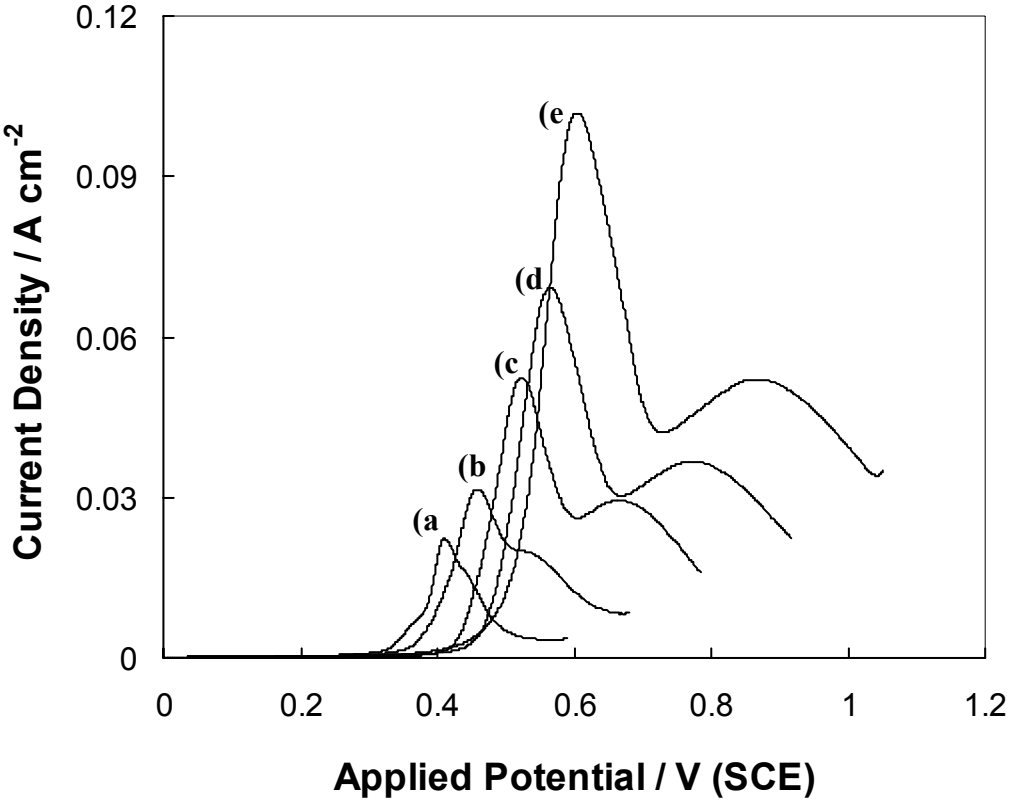

Fig. 4 Linear potential sweep of InP electrodes in 3 mol dm^{-3} KOH solution at scan rates of (a) 1 mV s^{-1}, (b) 2.5 mV s^{-1}, (c) 5 mV s^{-1}, (d) 7.5 mV s^{-1} and (e) 10 mV s^{-1}.

obtained for all scan rates but peak currents increase and values of potential at the peak shift in the anodic direction as the scan rate is increased. A secondary peak is also observed which becomes more clearly resolved at higher scan rates. The combined charge corresponding to both peaks was estimated by numerical integration of the current with respect to time. It appears that the variation in scan rate does not appreciably alter the quantity of charge passed, and a value of ~1.4 C cm^{-2} was measured for each scan rate.

Electrodes which have undergone a potential sweep as described for Fig. 4 clearly show the formation of porous InP in cross-sectional TEM as shown, for example, in Fig 1. Similar results are obtained in 2 mol dm^{-3} and 5 mol dm^{-3} KOH. Typical TEM cross-sections are shown in Fig 5. Similar results are also obtained under conditions of constant potential in 2 mol dm^{-3}, 3 mol dm^{-3} and 5 mol dm^{-3} KOH. However, in all

cases, a thin layer (~ 30 nm) close to the surface appears to be unmodified. The manner in which a porous region can form by electrochemical oxidation despite the presence of this dense InP layer at the surface is not apparent from Fig. 1. Closer examination by TEM, however, reveals the presence of pores through this dense near-surface layer. This can be seen in Fig. 5(a) and is illustrated more clearly in the TEM micrograph in Fig. 6 which shows a cross-section of an electrode which had been subjected to a potential sweep from 0.0 V to 0.825 V in 2 mol dm^{-3} KOH at a scan rate of 2.5 mV s^{-1}. It can be observed that the dense, near-surface layer appears to be penetrated at one point by a pore. This suggests a mechanism by which the porous layer can grow, *i.e.* it appears to be connected to the electrolyte by pores through the near-surface layer.

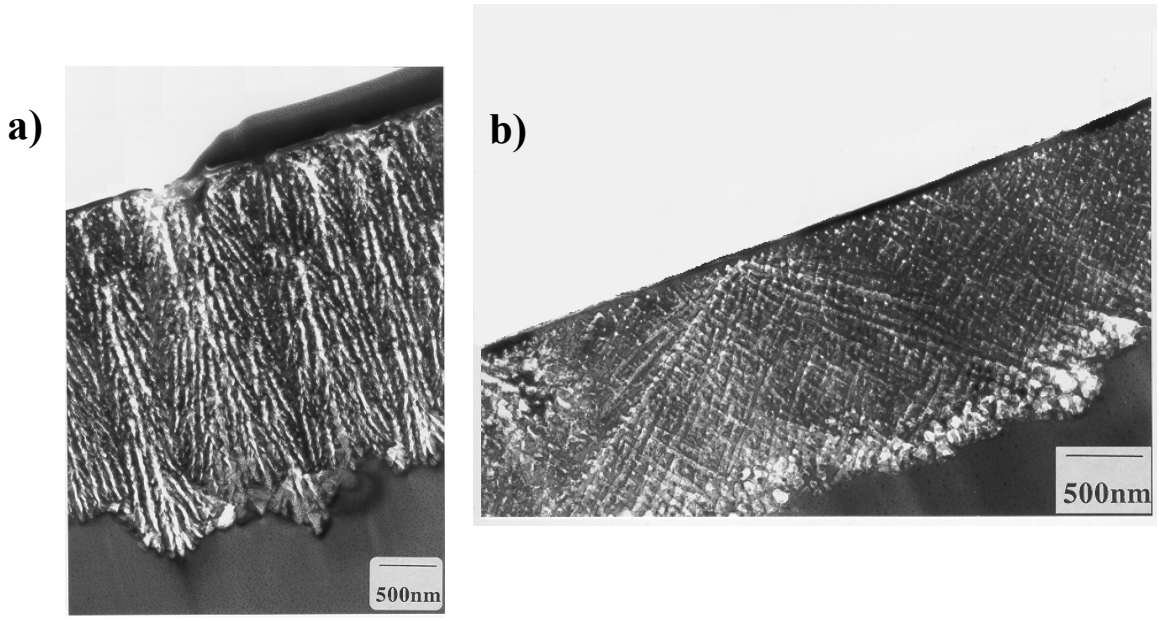

Fig. 5 (a) Bright field TEM of InP after a potential sweep from 0.0 V to 0.825 V (SCE) in 2 mol dm^{-3} KOH (b) Bright field TEM of InP after a potential sweep from 0.0 V to 0.675 V (SCE) in 3 mol dm^{-3} KOH. The potential sweep anodization was scanned at a rate of 2.5 mV s^{-1}. The plane of both micrographs is (110).

Further evidence for the existence of these pores was obtained from AFM observations of the surface of electrodes. Careful AFM examination of the surface of wafers after anodization shows the presence of pits in the surface. A typical pit can be seen in the AFM image in Fig. 7 which was obtained on an InP electrode that had been subjected to a potential sweep from 0.0 V to 0.7 V. Thus, it is believed that pits such as this penetrate the dense near-surface layer and act as pathways which connect the porous structure with the bulk electrolyte. It is assumed that both the porous layer and the pores through the near-surface layer are filled with electrolyte. This would enable ionic current to flow and electrochemical oxidation of InP to proceed, thus providing a mechanism by which the porous layer can grow.

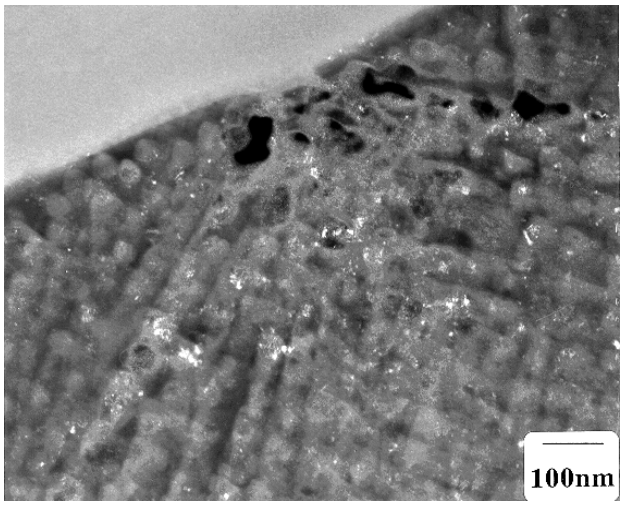

Fig. 6 Dark Field TEM of the porous InP cross-section after a potential sweep from 0.0 V to 0.825 V (SCE) in 2 mol dm^{-3} KOH at a scan rate of 2.5 mV s^{-1} showing etch pitting of the surface.

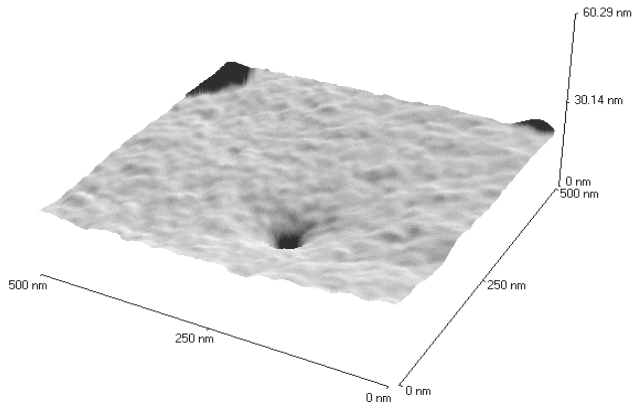

Fig. 7 AFM image obtained after the InP electrode was subjected to a potential sweep from 0.0 V to 0.7 V (SCE) in a 5 mol dm^{-3} KOH electrolyte at a scan rate of 2.5 mV s^{-1}.

The average thickness of the porous layers formed in 2, 3 and 5 mol dm^{-3} KOH after a potential sweep from 0.0 V to 0.825 V, 0.675 V and 0.7 V respectively, was measured from TEM micrographs. The mean pore width was also estimated approximately from each of these micrographs. It is clear that both the porous layer thickness and mean pore width decrease significantly with increasing concentration of KOH.

Potentiostatic anodization of n-InP electrodes at 0.9 V in 2, 3 and 5 mol dm^{-3} KOH also resulted in the formation of porous InP structures. The porous layers formed potentiostatically were similar to those formed under potential sweep conditions. The average thickness of porous layers formed after anodization at 0.9 V for 150 s in 2, 3 and

5 mol dm^{-3} KOH solutions were measured from TEM micrographs. Values of 2.38, 1.68 and 1.18 μm, respectively, were obtained showing a similar trend to that observed under potential sweep conditions.

For each of a series of samples for which the thickness of the porous layer was measured, the corresponding charge density passed was also estimated. This was done by estimating the integral of current with respect to time. The measured thickness of the porous layer was then plotted against the corresponding charge density. The results are shown in Fig. 8. It is clear that a good fit to a straight line though the origin is obtained. The slope of this line gives a value of 1.10 μm C^{-1} cm^2 for the ratio of porous layer thickness to charge density (Fig. 8 (a)). The observation that the porous layer thickness increases linearly with charge density indicates that a relatively constant percentage porosity is maintained.

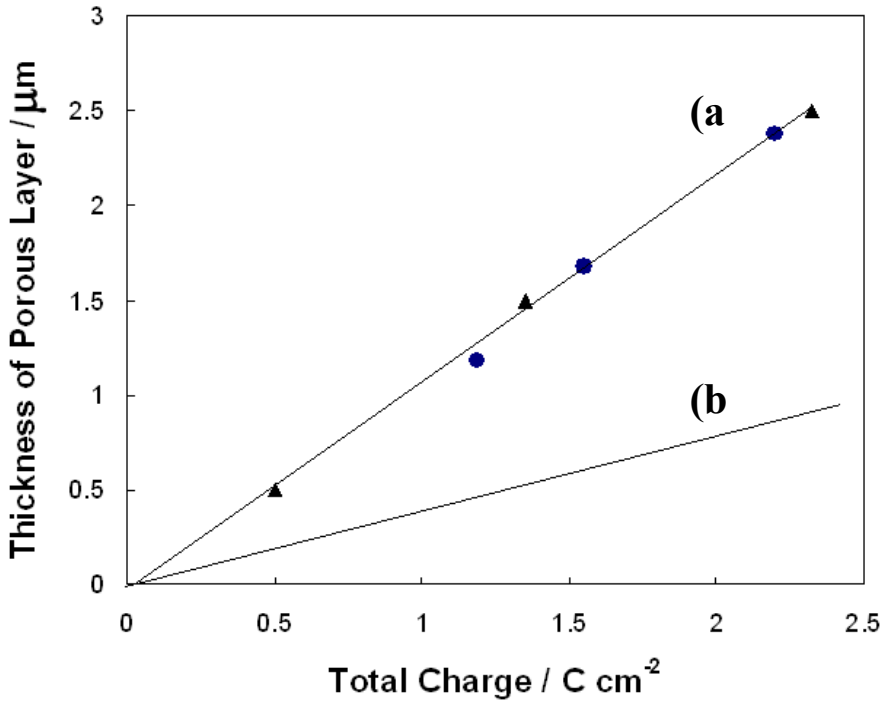

Fig. 8 Plot of porous layer thickness for samples anodized at constant potential (•) and after potential sweep (▲) as a function of the charge passed. (-) Theoretical thickness of InP removed.

Details of the mechanism of growth of porous layers are under investigation. The evidence presented here strongly suggests that the porous layer structure arises from the penetration of pits into the surface at particular points and pore propagation within the InP originating at these points. Presumably, the pores are filled with electrolyte, pore growth occurs at pore tips and the electrolyte within the porous structure is connected to the bulk electrolyte through the surface pits which penetrate the dense near-surface layer. Preliminary evidence suggests that pore growth may occur only along the <100> direction. The origin of the dense near-surface layer has not been fully explained but it is suggested that it may arise from carrier depletion in the semiconductor. The detailed electrochemistry also requires investigation.

Oscillatory Behavior

A typical linear sweep voltammogram at 300 mV s^{-1} for an n-InP electrode in 5 mol dm^{-3} aqueous KOH is shown in Fig. 9. Well-defined current oscillations are observed in the potential range 2.6 V to 3.0 V and have an average current density of ~0.5 A cm^{-2}. The voltammograms were found to have a similar oscillatory region for all the scan rates investigated (50 - 500 mV s^{-1}). Increasing the scan rate results in the shifting of the oscillatory region to more anodic potentials. Furthermore, the average current density of the oscillations is observed to increase with increasing scan rate.

Fig. 10 shows the current oscillations on an expanded potential axis. The current density of each oscillation increases with a progressively increasing slope up to a well defined current maximum followed by a sharp decrease to a well defined current minimum.

The period segment τ_1 is defined to be the time taken for the current to increase from a minimum value to a maximum value during an oscillation. The period segment τ_2 is defined as the time taken for the current to decrease from a maximum to a minimum in current during an oscillation. The total period of oscillation is then $(\tau_1 + \tau_2)$. For the purposes of studying the potential dependence, we define the potential of an oscillation as

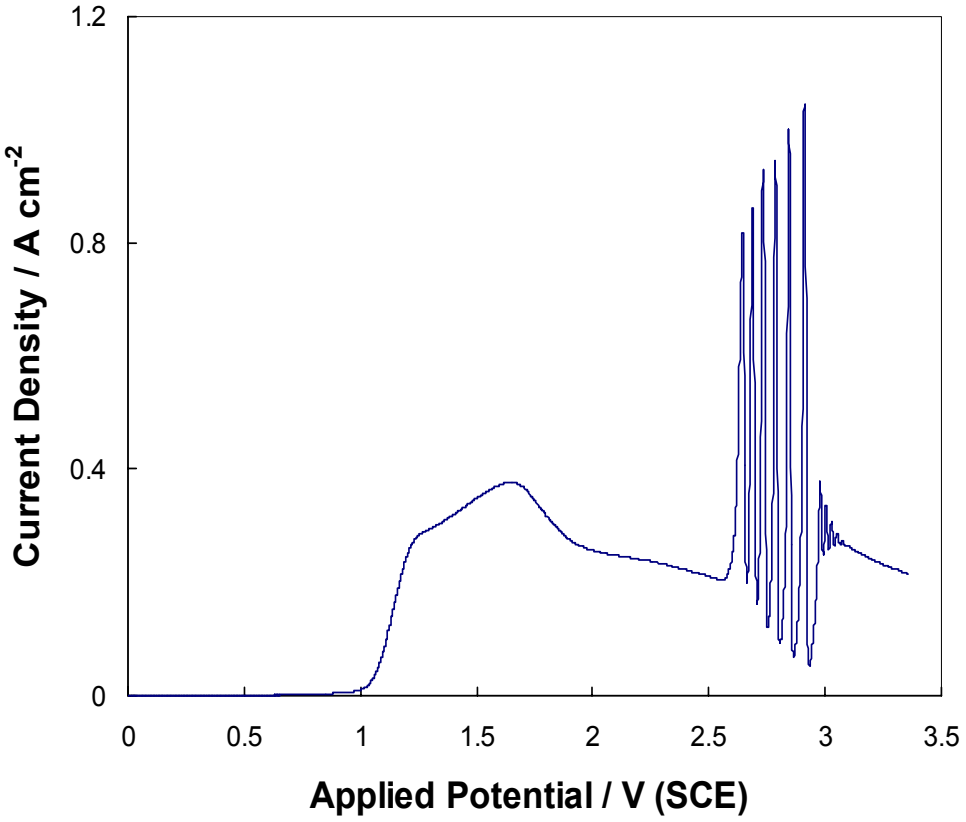

Fig. 9 Current density vs. potential curves of n-InP in 5 mol dm^{-3} KOH. The potential was scanned at 300 mV s^{-1} from 0.0 V to 3.4 V.

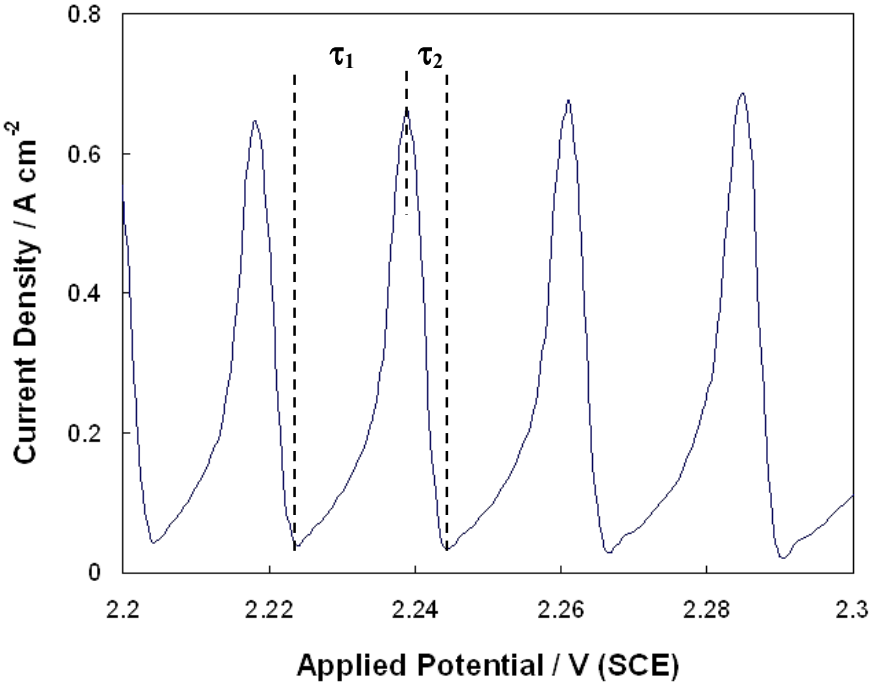

Fig. 10 Typical current oscillations observed during anodization of n-InP at a scan rate of 100 mV s^{-1} in 5 mol dm^{-3}. The potential axis has been expanded for clarity in the figure. The characteristic period segments τ_1 and τ_2 are shown.

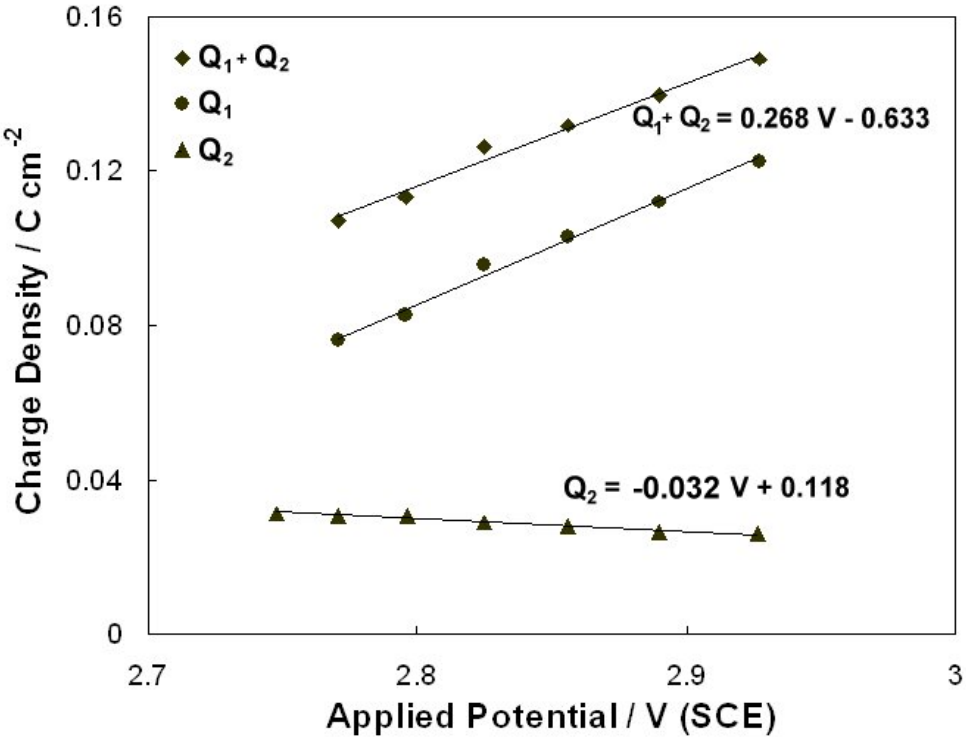

Fig. 11 Variation of the total charge per cycle ($Q_1 + Q_2$), charge associated with time τ_1 (Q_1) and charge associated with τ_2 (Q_2), as a function of potential.

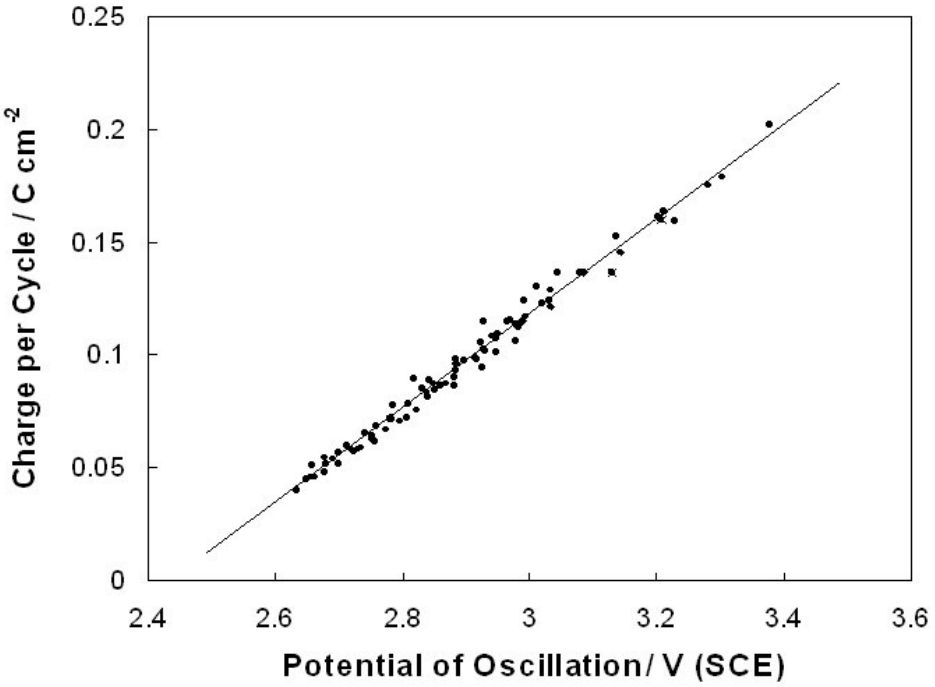

Fig. 12 Total charge per cycle plotted as a function of potential. The data was acquired from potential sweeps of n-InP in 5 mol dm^{-3} KOH with scan rates in the range 50 mV s^{-1} to 500 mV s^{-1}

the potential value at the current maximum for the oscillation. Investigation of the oscillatory region of linear potential sweeps obtained at scan rates in the range 50 mV s^{-1} to 500 mV s^{-1} revealed that the oscillation profile retains the same form as that shown in Fig. 2, regardless of the scan rate.

The charge passed during each oscillation was estimated by numerical integration of the current with respect to time. This was done for each oscillation in a potential sweep. The charge per oscillation was plotted against the potential of the oscillation and a typical plot is shown in Fig. 11. The charge associated with the segments τ_1 and τ_2 are also plotted (Q_1 and Q_2 respectively). The total charge per cycle ($Q1 + Q_2$) increases with increasing potential and a rate of approximately 0.268 C cm^{-2} V^{-1} is obtained from the slope of the linear fit to the data. The charge passed during the time segment τ_1 also increases linearly with increasing potential, whereas the charge passed during the time segment τ_2 decreases slightly as the potential increases. The segment, τ_1, is observed to represent the major portion of the total charge per cycle, whereas the charge associated with segment τ_2 is relatively constant with a measured decrease of 0.032 C cm^{-2} V^{-1}.

The charge per cycle was also estimated by numerical integration for the series of potential sweeps with scan rates in the range of 50 mV s^{-1} to 500 mV s^{-1}. This data was plotted as a function of the potential of oscillation and a linear dependence was observed as shown in Fig. 12. The slope of the linear fit yields a value of 0.216 C cm^{-2} V^{-1} for the increase in the charge per cycle with potential. It is noted that, as the scan rate increases, the range of the oscillatory region is shifted to higher potentials. The composite data set (represented in Fig. 5) therefore includes a larger overall range of potential and the charge per cycle is a well-behaved linear function of potential over this expanded range.

Current oscillations are also observed when n-InP electrodes are anodized in 3 mol dm^{-3} $(NH_4)_2S$ solution [7,23,24]. However, the oscillations observed under potential sweep conditions in the sulfide electrolyte have a fairly symmetrical waveform, as shown in Fig. 13 with a sinusoidal appearance and with $\tau_1 \cong \tau_2$ over the whole potential range. This contrasts sharply with the waveform observed in the KOH electrolyte.

The charge per cycle, acquired from numerical integration of the current over time, for InP electrodes anodized at various scan rates in 3 mol dm^{-3} $(NH_4)_2S$, is found to be constant and has a value of 0.32 C cm^{-2}. Thus, as the potential increases in a potential sweep, the current increases correspondingly and the charge per cycle remains constant, implying that the period of oscillation must decrease proportionately. Within the ranges studied, the charge per cycle remains constant irrespective of solution concentration, pH and scan rate for both potentiodynamic and potentiostatic anodization.

The exact mechanism of the oscillatory behavior is still under investigation. It may be related to the presence of a porous layer on the surface, since this is observed in both KOH and $(NH_4)_2S$ electrolytes and possibly involves periodic inhibition of processes at the electrode surface, due either to cyclic electrolyte depletion or the anodic growth and dissolution of a passivating film at the interface.

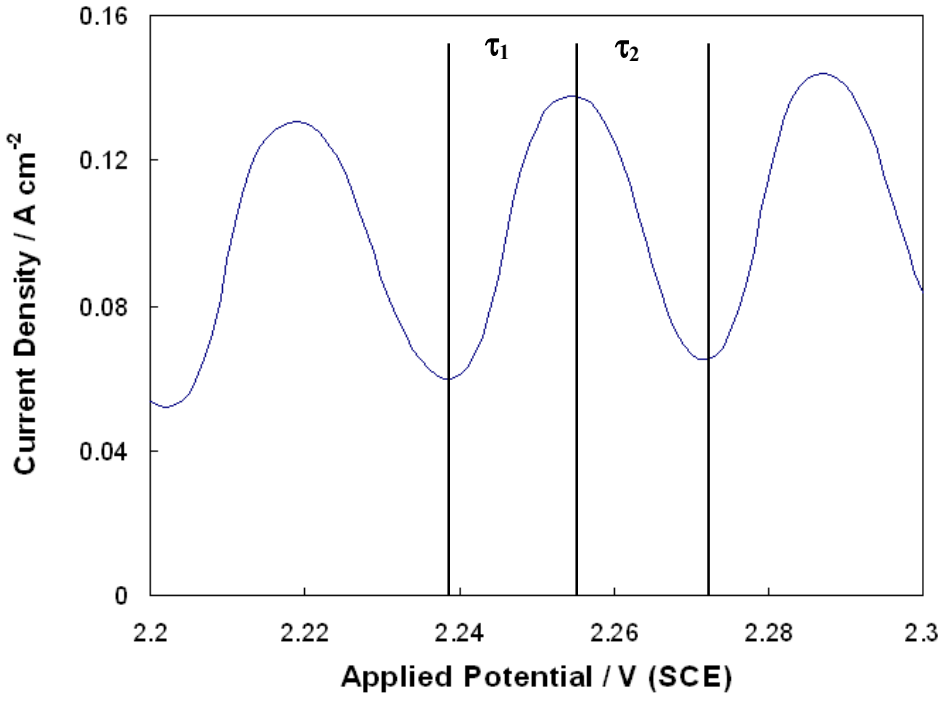

Fig. 13 Typical current oscillations observed during a linear potential sweep of n-InP in 3 mol dm^{-3} $(NH_4)_2S$ at a scan rate of 10 mV s^{-1}. The potential axis has been expanded for clarity in the figure. The characteristic period segments τ_1 and τ_2 are shown.

CONCLUSION

The anodic oxidation processes are remarkably different in different concentrations of KOH. Anodization in 2 - 5 mol dm^{-3} KOH results in the formation of porous InP layers but, under similar conditions in 1 mol dm^{-3} KOH, no porous structure is evident. Rather, the InP electrode is covered with a thin, compact, surface film at lower potentials and, at higher potentials, a highly porous surface film is formed which cracks on drying.

Anodization of electrodes in 2 - 5 mol dm^{-3} KOH results in the formation of porous InP under both potential sweep and constant potential conditions. The porosity is estimated at ~65%. A thin layer (~ 30 nm) close to the surface appears to be unmodified. It is observed that this dense, near-surface layer is penetrated by a low density of pores. This suggests a mechanism by which the porous layer can grow, *i.e.* it appears to be connected to the electrolyte by pores through the near-surface layer. The mechanism is discussed in more detail elsewhere in this volume [25].

Well defined oscillations are observed when InP is anodized in both the KOH and $(NH_4)_2S$. In the InP/$(NH_4)_2S$ system the oscillations have a fairly symmetric profile. In contrast, the oscillations observed in the InP/KOH case exhibit an asymmetrical current vs. potential profile. While the charge per cycle remains constant at 0.32 C cm^{-2} in $(NH_4)_2S$ irrespective of the value of the applied potential, in the KOH system the charge per cycle increases linearly with potential. Thus, while the characteristics of the oscillations in the two systems investigated are dissimilar in many ways, both show reproducible and well-behaved values of charge per cycle. The exact mechanism of the oscillatory behavior is still under investigation.

REFERENCES

[1] I. Gerard, N. Simon and A. Etcheberry, *Appl. Surf. Sci.*, **175-176**, 734 (2001)

[2] P. Schmuki, G.I. Spoule, J.A. Bardwell, Z.H. Lu and M.J. Graham, *J. Appl. Phys.*, **79**, 7303 (1996)

[3] J. Yota and V.A. Burrows, *J. Vac. Sci. Technol. A*, **11**, 1083 (1993)

[4] Z.S. Li, X.Y. Hou, W.Z. Cai, W.Wang, X.M. Ding and X. Wang, *J. Appl. Phys.,* **78**, 2764 (1995)

[5] L.J. Gao, J.A.Bardwell, Z.H. Lu, M.J. Graham and P.R. Norton, *J. Electrochem. Soc.*, **142**, L14 (1995)

[6] E. Harvey, D.N. Buckley, S.N.G. Chu, D. Sutton and S.B. Newcomb, *J. Electrochem. Soc.*, **149** (Sept. 2002)

[7] D.N. Buckley, E. Harvey and S.N.G. Chu, *Chemical Monthly*, **133**, 785 (2002)

[8] E. Harvey and D.N. Buckley, in *Proceedings of the 32nd State-of-the-Art Program on Compound Semiconductors*, R.F. Kopf, A.G. Baca and S.N.G. Chu, Editors, PV 2000-1, p. 265, The Electrochemical Society, Proceedings Series, Pennington, NJ (2000)

[9] L.-H. Peng, C.-H. Liao, Y.-C. Hsu, C.-S. Jong, C.-N. Huang, J.-K. Ho, C.-C. Chiu and C.-Y. Chen, *Appl. Phys. Lett.*, **76**, 511 (2000)

[10] F.M. Ross, G. Oskam, P.C. Searson, J.M. Macaulay and J.A. Liddle, *Philos. Mag. A*, **75**, 2 (1997)

[11] E. Harvey, C. O'Dwyer, T. Melly, D.N. Buckley, V.J. Cunnane, D. Sutton, S.B. Newcomb and S.N.G. Chu, in *Proceedings of the 35th State-of-the-Art Program on Compound Semiconductors*, P.C. Chang, S.N.G. Chu, and D.N. Buckley, Editors, PV 2001-2, p. 87, The Electrochemical Society, Proceedings Series, Pennington, NJ (2001)
[12] M.M. Faktor, D.G. Fiddyment and M.R. Taylor, *J. Electrochem. Soc.*, **122**, 1566 (1975)
[13] D.J. Lockwood, P. Schmuki, H.J. Labbé, J.W. Fraser, *Physics E*, **4,** 102 (1999)
[14] X.G. Zhang, S.D. Collins, R.L. Smith, *J. Electrochem. Soc*., **136,** 1561 (1989)
[15] J.S. Shor, I. Grimberg, B.-Z. Weiss and A.D. Kurtz, *Appl. Phys. Lett.*, **62,** 2836 (1993)
[16] A. Uhlir, Jr., *Bell System Tech. J.*, **35**, 333 (1956)
[17] P. Schmuki, J. Fraser, C.M. Vitus, M.J. Graham, H.S. Isaacs, *J. Electrochem. Soc.*, **143**, 3316 (1996)
[18] P. Schmuki, D.J. Lockwood, J. Fraser, M.J. Graham, H.S. Isaacs, *Mater. Res. Soc. Symp. Proc.,* **431**, 439 (1996)
[19] M. Christopherson, J. Carstensen, A. Feuerhake and H. Föll, *Mater. Sci. Eng. B*, **69**, 70, 194 (2000)
[20] S. Rönnebeck, J. Carstensen, S. Ottow and H. Föll, *Electrochem. Solid-State Lett.*, **2**, 126 (1999)
[21] P. Schmuki, L.E. Erickson, D.J. Lockwood, J.W. Fraser, G. Champion, H.J. Labbé, *Appl. Phys. Lett.*, **72,** 1039 (1998)
[22] O. Pluchery, J. Eng Jr., R.L. Opila and Y.J. Chabal, *Surf. Sci.*, **502**, 75 (2002)
[23] E. Harvey and D.N. Buckley, *Electrochem. Solid-State Lett.*, **5**, G22 (2002)
[24] D.N. Buckley, E. Harvey and S.N.G. Chu, in *Proceedings of the State-of-the-Art Program on Compound Semiconductors XXXVI and Wide Bandgap Semiconductors for Photonic and Electronic Devices and Sensors III*, R.F. Kopf, F. Ren, E.B. Stokes, H.M. Ng, A.G. Baca, S.J. Pearton and S.N.G. Chu, Editors, PV 2002-3, p.286, The Electrochemical Society, Proceedings Series, Pennington, NJ (2002)
[25] C. O'Dwyer, D. N. Buckley, D. Sutton, M. Serantoni and S. B. Newcomb, *This Volume*, A Mechanistic Study of Anodic Formation of Porous InP